M.Tech (Geotechnical Engineering)

Neha Pawar (23/GTE/03)

2025

EVALUATION OF DAMAGE AND FLOW IN REINFORCED GEOMATERIAL SUBJECTED TO VIBRATORY LOADS

MAJOR PROJECT REPORT

A Dissertation Submitted

in Partial Fulfillment of the Requirements for the Degree of

MASTER OF TECHNOLOGY

IN

GEOTECHNICAL ENGINEERING

BY:

Neha Pawar

(2K23/GTE/03)

Under the Supervision of

Prof. Ashutosh Trivedi

Professor

Delhi Technological University

Department of Civil Engineering

DELHI TECHNOLOGICAL UNIVERSITY

(Formerly Delhi College of Engineering)

Shahbad, Daulatpur, Main Bawana Road, Delhi-110042

May, 2025

EVALUATION OF DAMAGE AND FLOW IN REINFORCED GEOMATERIAL SUBJECTED TO VIBRATORY LOADS

MAJOR PROJECT REPORT

A Dissertation Submitted

in Partial Fulfillment of the Requirements for the Degree of

MASTER OF TECHNOLOGY

IN

GEOTECHNICAL ENGINEERING

BY:

Neha Pawar

(2K23/GTE/03)

Under the Supervision of

Prof. Ashutosh Trivedi

Professor

Delhi Technological University

Department of Civil Engineering

DELHI TECHNOLOGICAL UNIVERSITY

(Formerly Delhi College of Engineering)

Shahbad, Daulatpur, Main Bawana Road, Delhi-110042

May, 2025

DELHI TECHNOLOGICAL UNIVERSITY

(Formerly Delhi College of Engineering)
Shahbad Daulatpur, Main Bawana Road, Delhi-110042

CANDIDATE'S DECLARATION

I, Neha Pawar (2K23/GTE/03) student of MTech, Geotechnical Engineering, hereby declare that the project dissertation entitled **"Evaluation of damage and flow in reinforced geomaterial subjected to vibratory loads"** which is submitted by me to the Department of Civil Engineering, Delhi Technological University, Delhi in partial fulfilment of the requirement for the award of the degree of Master of Technology, is original and not copied from any source without proper citation. This work has not previously formed the basis for the award of any degree, diploma associateship, fellowship or other similar title or recognition.

Place: Delhi **Neha Pawar**

Date:

DEPARTMENT OF CIVIL ENGINEERING
DELHI TECHNOLOGICAL UNIVERSITY
(Formerly Delhi College of Engineering)
Shahbad Daulatpur, Main Bawana Road, Delhi-110042

CERTIFICATE

I hereby certify that the Project Dissertation titled **"Evaluation of damage and flow in reinforced geomaterial subjected to vibratory loads"** which is submitted by Neha Pawar (2k23/GTE/03) Department of Civil Engineering, Delhi Technological University, Delhi in partial fulfilment of the requirement for the award of the degree of Master of Technology, is a record of the project work carried out by the students under my supervision. To the best of my knowledge this work has not been submitted in part or full for any degree or diploma to this university or elsewhere.

This is to certify that the student has incorporated all the corrections suggested by the examiners in the thesis and that the statement made by the candidate is correct to the best of our knowledge.

Place: Delhi **(Prof. A. Trivedi)**
Date: Supervisor

(Signature of Examiner)

ABSTRACT

In the present study, a series of numerical and experimental simulations have been carried out to investigate the flow of the geomaterial in confined state. The finite element modelling in a commercialized software package Abaqus was then carried out to investigate the flow characteristics of confined geomaterial subjected to vibratory loads. The increase of friction angle and load shows a drop in the magnitude of flow shearing stresses. A model testing was then carried out to investigate the characteristics of waves in term of voltage output. The damage and flow in terms of stiffness capacity with penetration has been evaluated for the confined geomaterial subjected to vibratory loads. The CBR method has been used to capture the stiffness capacity and penetration factor for the selected set of geogrid reinforcements. The stiffness capacity (0.95) of unreinforced and geogrid reinforced sections have been substantiated with stiffness capacity for jute reinforcement sections. It has been observed that geogrid reinforcement enhances the stiffness capacity of the geomaterial matrix in contrast to jute and unreinforced sections. Moreover, the three layers of geogrid effectively dampens the stress waves and likely to be a reason for improved stiffness capacity. The findings from the presented investigations implies that the proposed concept of flow geomaterial is very crucial geostructures and likely to open a new avenue of research in the field of confined geomaterial dynamics.

ACKNOWLEDGEMENT

It is with great appreciation that I thank all those who were involved with the work presented in this report.

My first thanks go to my supervisor, Prof. Ashutosh Trivedi, for his support and critical appraisal which helped me in completing my research work. Their expertise helped in the growth of this work, and their support was unwavering.

Also, I would like to extend my gratitude to Mr. Yakshansh Kumar for assisting with the collection of data and experiments and analysis that aided me to effectively complete this research.

At the same time, I thank Delhi Technological University for giving me the chance to get the materials and facilities which were needed for the project.

Last but not least, I send my familiarization to the family for all the overriding affection, care, and patience as well as their strength. Their expectations for me have been useful most of the time and at critical periods of this journey.

NEHA PAWAR

Roll No. 2K23/GTE/03

Department Of Civil Engineering

Delhi Technological University

TABLE OF CONTENT

LIST OF TABLES

LIST OF FIGURES

LIST OF SYMBOLS, ABBREVIATIONS, AND NOMENCLATURE

ϕ: angle of internal friction

c: cohesion

τ: shear stress at failure

σ: normal stress applied

FEA: Finite element analysis

Fig.: Figure

$\delta\varepsilon_h$: horizontal strain

$\delta\varepsilon_z$: vertical strain

δ_γ: yielding strain

$\delta\varepsilon$: elastic strain

f: flow

Ψ: angle of dilation

ε_{ij}: total strain

$\varepsilon^p{}_{ij}$: plastic strain,

σ_3: major principal stress

σ_1: minor principal stress

k: stiffness

k_{max}: maximum stiffness

CHAPTER 1

INTRODUCTION

The evaluation of deformation, stress-strain, and damping characteristics of flow in reinforced geomaterial subjected to vibratory loads is very crucial while analyzing and designing the systems supported by earth structures (Kumar et al., 2025). This is particularly applicable for the systems subjected to repetitive or dynamic vibrations, namely highway traffic, railways, industrial machinery, or seismic loads (El-Khoury et al., 2013). The geomaterials are susceptible to progressive damage under repeated vibratory loading which imparts effect on durability and long-term integrity of the geostructures (Zhang et al., 2022). The present study explores the damage and flow characterization in geomaterials under vibratory loading using numerical and experimental testing. The numerical analysis is carried out using sophisticated finite element method (FEM) to model the vibratory loading conditions and simulate the measured damage processes. The flow behavior is investigated in the numerical model via detailed examination of stress distribution, strain localization, and damage accumulation with time. To overcome the shortcoming of the unpaved surface a model testing is conducted, in which reinforced and unreinforced samples of geomaterial are tested under various frequencies and amplitudes of vibratory loading. As per the research conducted, an MS steel tank is taken in which cohesionless geomaterial is filled to carry out the analysis. All the work done is in reinforced geomaterial subjected to vibratory loads and its evaluation of damage and flow is concluded. After model testing, an experimental testing is also carried out which is one of the primal aims to study the reinforcement of geogrids in the matrix of geomaterial to investigate its influence on the stiffness capacity and damping. Geogrids are employed to improve the strength and confining pressure of the geomaterial that possess the potential to slow down damage and reduce the rate of degradation under vibratory loading (Sweta et al., 2022). The role of geogrids is to put a systematic trial by comparing reinforced and unreinforced samples under identical testing conditions. Reinforced geomaterial is a material or method used to regulate or limit the movement of granular materials, typically geomaterial or geomaterial like mixtures within a specific area.

CHAPTER 2

LITERATURE REVIEW

Geosynthetic material has been introduced as a crucial material in geotechnical engineering as it enhances the performance of geomaterial under static and dynamic loading conditions. The major application areas include unpaved roads, foundations, buried pipelines, and seismic isolation systems. The geosynthetics (like geogrid) are applied in geomaterials to improve load-bearing capacity, deformation control, stiffness, and energy dissipation due to vibratory loads. The evaluation of rut pattern in unreinforced and reinforced geomaterial using full-scale moving wheel load tests disclosed the enhanced load distribution and reduced surface deformation due to the inclusion of geogrid reinforcement (Singh et al., 2022). The application of natural jute fibers was seen as a sustainable reinforcement in cohesionless pavement materials, and significant enhancements in stiffness characteristics were found for varied depths of jute reinforcement (Kumar et al., 2023). The behaviour of shallow foundations on reinforced sand under vertical loading, increased bearing capacity, and reduced settlements was established (Kirtimayee et al., 2022). The study on geogrid-cased granular pile anchors was performed in cohesionless geomaterials, and the key factors that influenced their performance were identified, namely, pile configuration and geomaterial density (Bajaj et al., 2022). In terms of structural systems, the mechanical behaviour of soil pipe systems and geosynthetic reinforcement was examined, resulting in the reinforcement improving stress distribution and improving the structural integrity of embedded pipes (Pires et al., 2021). The strength of copper slag (a byproduct) was explored as a structural fill in reinforced geomaterial structures, indicating its feasibility from both mechanical and environmental perspectives (Prasad et al., 2016). Evolution in dynamic testing methods has significantly engaged in characterizing geomaterials under cyclic and seismic loading. The impact of the centrifuge model was highlighted with boundaries and loading characteristics on the evaluation of dynamic properties in dry cohesionless geomaterial (Tsai et al., 2021). Torsional and flexural resonant column testing of grouted cohesionless geomaterials was conducted to reveal the influence of grouting on stiffness and damping (Basas et al., 2020). The importance of

specimen size and inertial effects in resonant column testing provides insight into the reliability of the test (Vrettos et al., 2022). The utilization of large amplitude oscillatory shear tests was carried to investigate the non-linear dynamic properties of ultrasoft cohesive geomaterial (Wang et al., 2023), while the horizontal dynamic response of partially embedded were studied for piles in dry geomaterials under combined loading conditions (Zou et al., 2023). Nowadays, geomaterial structure interaction has also become a key area of interest in enhancing infrastructure resilience. Dynamic soil structure interaction influences the behaviour of railroad frame bridges, emphasizing the need for modelling in the seismic design (Heiland et al., 2023). The dynamic behaviour of jointed rock masses using cyclic triaxial tests was investigated, providing valuable data on vibration characteristics in fractured geological settings (Peellage et al., 2022). Moreover, the wavelet transform techniques were employed to determine damping ratios in lacustrine soils, demonstrating the growing integration of advanced signal processing methods in geotechnical analysis (Fernandez-Lavin et al., 2024).

2.1. Research gaps

a) The available studies include limited integration of natural and sustainable reinforcements. There is a requirement for experimental and numerical studies analyzing the long-term durability, damping properties, and resilience of geosynthetic materials in real-world conditions.
b) Understanding of the soil geosynthetic interface under variable dynamic conditions is insufficient. More research work is needed on the behaviour of reinforced systems under fluctuating loading conditions.
c) The exploration of multi-axis and combined load effects on reinforced systems is limited, and a more robust investigation into 3D load interactions and failure mechanisms is necessary.

2.2. Objective

a) To evaluate the deformation and flow produced by the vibratory loads in geomaterial using numerical analysis.

b) To obtain shear modulus from stress-strain characteristics evaluated by damage and flow in geomaterial subjected to vibratory loads.
c) To determine the dynamic characteristics of confined geomaterial using piezo sensors and geogrid.
d) To investigate the dynamic characteristics, namely, damping of confined geomaterial surface reinforced with geogrid using piezoelectric output of PZT patches.
e) To estimate the performance of geogrid and jute reinforcement by the parameters such as stiffness capacity and penetration factor.

CHAPTER 3

MATERIAL AND METHODS

3.1. Material

Cohesionless geomaterials and geogrid reinforcement, as considered in the present work, are often used in the construction of transportation networks. Cohesionless geomaterials have no electrochemical bonding between particles and instead depends mostly upon internal friction and particle interlock for shear strength. This renders their mechanical response extremely sensitive to parameters, namely, particle size distribution, relative density, moisture content, and compaction effort. As the main load-bearing medium when used in unpaved road construction, these geomaterials carry wheel loads down to the underlying subgrade.

3.2. Method

The index properties tests allow engineers to classify and characterize the soil for its specific construction purposes. Understanding the particle size distribution helps in determining whether a geomaterial can bear the weight of moving traffic over pavement, and the Atterberg limits help identify whether the soil will be prone to significant shrinkage or expansion. Moisture content and compaction tests are essential for ensuring that the soil provides a stable base for construction activities. The knowledge gained from these experiments forms the basis for more advanced testing and design decisions, such as those involving dynamic load analysis, reinforced pavement design, or geotechnical engineering for geostructure construction. As per the IS code guidelines, the listed experiments are performed to identify the type and behaviour of the geomaterial. Table I represents the experiments performed as per the IS code for the index properties of geomaterial.

Table 1: List of experiments conducted for the determination of basic index and advanced geomaterial properties

S.No.	Experiments	Properties	Indian standards
1.	Particle size distribution	Soil gradation	IS 2720: Part 4 (1985)
2.	Standard proctor test	OMC and MDD	IS 2720: Part 7 (1980)
3.	California bearing ratio test	CBR value, stiffness capacity, penetration factor	IS 2720: Part 16 (1987)
4.	Direct shear test	Angle of friction and cohesion	IS 2720: Part 13 (1986)

1) Grain size distribution

The distribution of the grain size of the geomaterial was measured by sieve analysis (IS 2720: Part 4, 1985). The geomaterial sample was oven-dried and subjected to a series of standard sieves placed in decreasing order of their mesh sizes. The weight of the retained particles on each of the sieves was recorded, and the particle size distribution curve was drawn. The test involves passing 1 kg of oven-dried geomaterial through a stack of standard IS sieves (4.75 mm, 2 mm, 1 mm, 600 μm, 300 μm, 150 μm, 75μm and pan). The geomaterial retained on each sieve is weighed to calculate the percentage retained and the cumulative percentage passing.

$$Percentage\ retained = \frac{Weight\ retained}{Total\ sample\ weight} \times 100 \quad \text{.....(1)}$$

$$Percentag\ passing = 100 - Cumulative\ percentage\ retained \quad \text{.....(2)}$$

The particle size distribution curve is then plotted with grain size (log scale) on the x-axis and percentage finer (passing) on the y-axis. This curve helps in determining the uniformity coefficient (C_u) and the coefficient of curvature (C_c):

$$C_u = D_{60}/D_{30} \quad \text{.....(3)}$$

$$C_c = \frac{(D^{30})^2}{D_{10} \times D_{60}} \quad \text{.....(4)}$$

where D_{10}, D_{30}, and D_{60} are the diameters of the particle corresponding to 10, 30, and 60% finer, respectively.

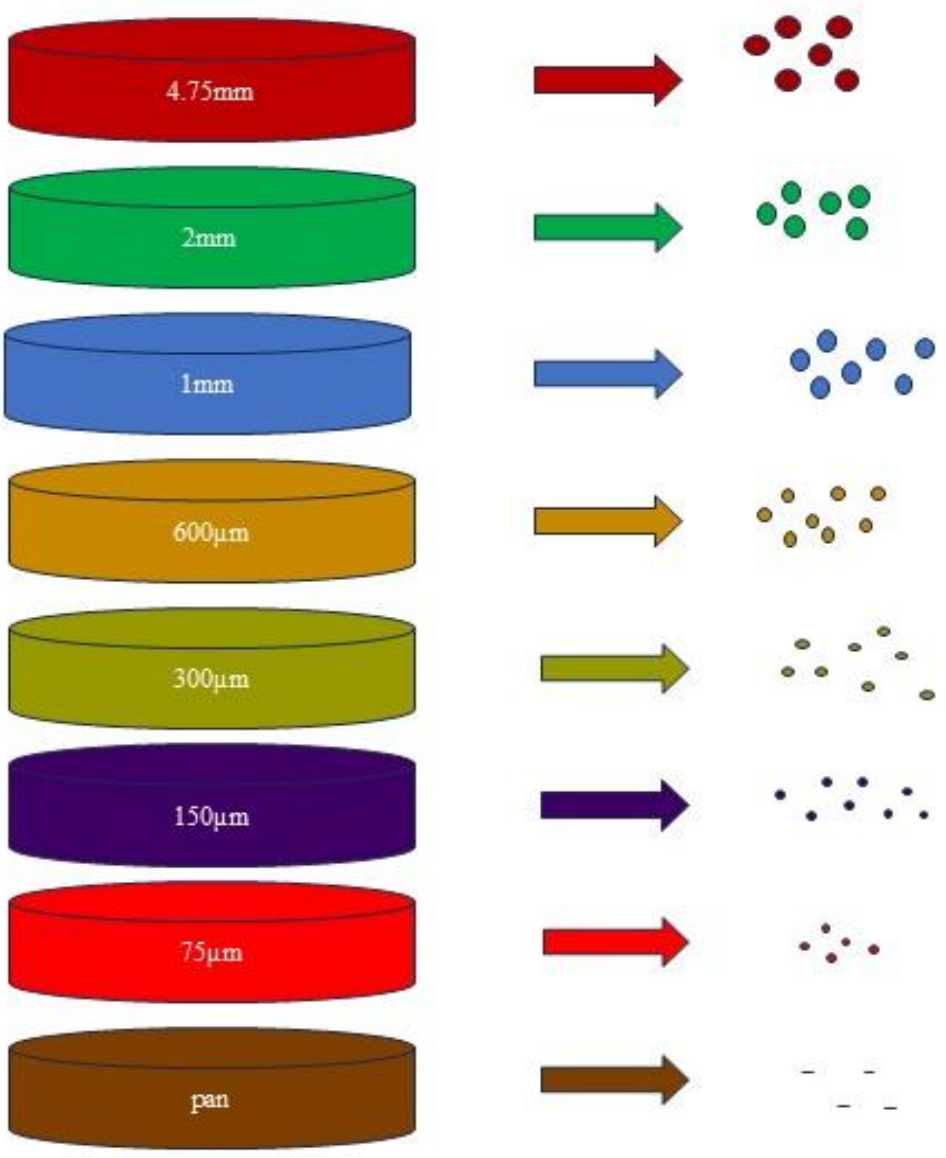

Figure 1: Artistic representation of the grain size analysis of geomaterial passing through 4.75-0.075 mm sieves

2) Standard proctor compaction test

Standard proctor test was conducted to obtain the optimum moisture content (OMC) and maximum dry density (MDD) of the geomaterial (IS 2720: Part 7, 1980). Geomaterial samples were compacted in a standard mold, imparting twenty-five blows from a standard rammer. Multiple tests were performed at varying moisture contents, and the corresponding dry densities were graphed to determine the OMC and MDD.

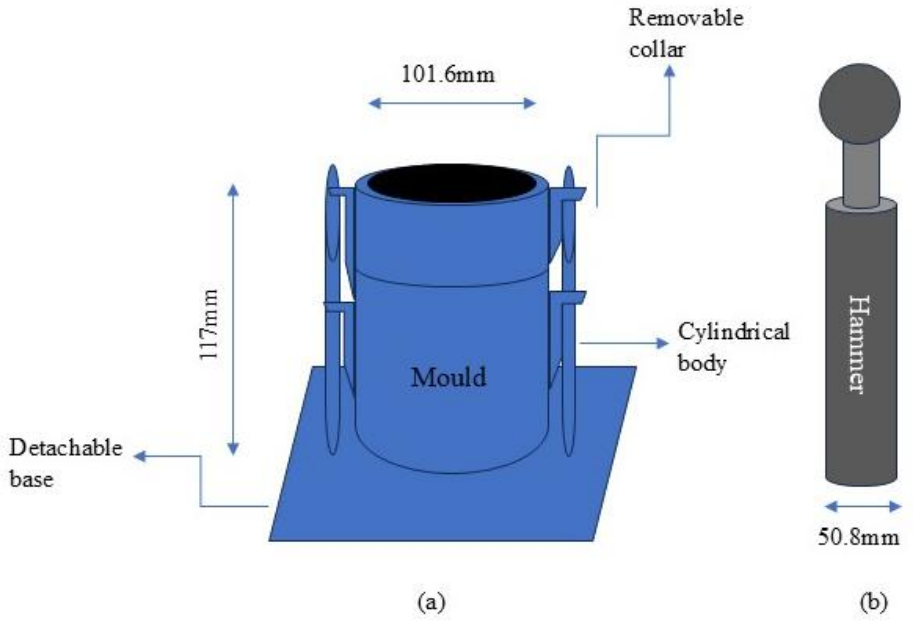

Figure 2**:** Diagrammatic representation of (a) the mould and (b) the hammer used to conduct the standard proctor test

The geomaterial samples was compacted in a 1000 cc proctor mold in three equal layers using a 25.5 kN rammer dropped from a height of 310 mm (25 blows per layer). The geomaterial samples were prepared with varied moisture content. The weight and moisture content of each sample were measured to calculate dry density as detailed below:

$\gamma = W/V$ .....(5)

$\gamma_d = \gamma/(1 + w)$ .....(6)

where γ is bulk unit weight, γ_d is the dry unit weight, W is the weight of compacted geomaterial, V is the volume of mold, and w is the moisture content

3) California Bearing Ratio (CBR) Test

The CBR test (IS 2720: Part 16, 1987) consists of compacting the geomaterial in a mold at OMC, wetting it for 96 hours, and subsequently subjecting it to a standard load using a plunger at a uniform rate. The pressure needed to penetrate the geomaterial is recorded, and the CBR value is obtained as a percentage of the pressure needed to make the same penetration in a standard crushed rock specimen. A plunger of 50 mm diameter is penetrated into the sample at 1.25 mm/min, and the load corresponding to 2.5 mm and 5 mm penetrations is recorded.

$$CBR = \frac{Test\ load\ at\ penetration}{Standard\ load} \times 100 \quad \text{.....(7)}$$

The standard loads are:

- 13.5×10^3 kN for 2.5 mm penetration
- 20.16×10^3 kN for 5.0 mm penetration

The higher of the two CBR values is reported as the CBR value.

4) Direct Shear Test

The direct shear test was performed to ascertain the shear strength parameters, namely, the angle of internal friction (ϕ) and cohesion (c) (IS 2720: Part 13, 1986). A soil sample (60 mm × 60 mm × 25 mm) is placed in a shear box, which is split into two halves. Normal load is applied, and one half of the box is moved laterally at a constant rate to induce shear. The shear force and corresponding displacement are recorded until the sample fails. Fig. 3 represents the shear box, which is used in the direct shear test to perform the experiment.

$$\tau = c + \sigma.tan\phi \quad \text{.....(8)}$$

where, τ is the shear stress at failure, σ is the normal stress applied, c is cohesion, φ is angle of internal friction.

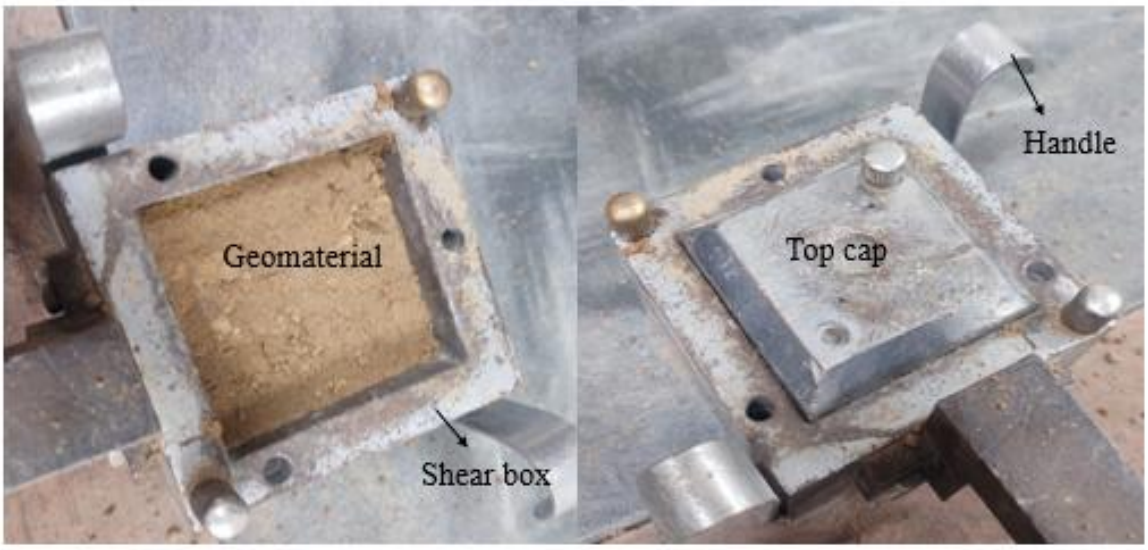

Figure 3**:** Pictorial representation of (a) the shear box filled with geomaterial and (b) the apparatus before placing in the load frame of shear box

The geomaterial properties for the sample under investigation are presented in Table II, derived from tests conducted in the laboratory. To evaluate the stiffness characteristics of the geomaterial, the California Bearing Ratio (CBR) test was performed. Initially, the CBR test was conducted under unsoaked conditions, followed by testing under soaked conditions. In accordance with IS: 2720 Part-6 (1987), standard apparatus and dimensions were employed. The cylindrical mold used for the CBR test has a diameter of 150 mm and a height of 175 mm, with an attached base plate. The collar height is 50 mm. The compaction rammer, with a weight of 24.525 kN and a diameter of 147 mm, has a net capacity of 2250×10^{-9} m^3. CBR values for both unreinforced and geogrid-reinforced geomaterial samples were determined based on plunger penetration measurements at 2.5 mm and 5 mm. The testing procedure involved applying a load to the top surface of the sample via a plunger at a constant rate of penetration (1.25 mm/min). A soaked sample is shown in Fig. 4, which is soaked for 96 hours. This test is essential for determining the strength and bearing capacity of the geomaterial.

Table II: Properties of geomaterial obtained from experiments conducted

S.no.	Property	Value	Units
1.	Specific gravity, G	2.63	-
2.	Optimum moisture content, OMC	12.32	%
3.	Maximum dry unit weight, MDD	19.57	kN/m^3
4.	Type of soil	SW	-
5.	CBR value	8.34	%
6.	Cohesion, c	Zero	kN/m^2
7.	Angle of friction, ϕ	32	Degrees

CHAPTER 4

FINITE ELEMENT MODELLING

In geotechnical engineering, numerical modeling is an important tool to understand the behavior of geomaterials under different conditions. In this research, a finite element model with the help of the software ABAQUS to model geomaterial behaviour based on data from previous experimental work was carried out. The model utilizes a number of geotechnical parameters based on laboratory test results, such as specific gravity, optimum moisture content (OMC), maximum dry density (MDD), angle of internal friction, and cohesion. Fig. 4 shows the steps followed in simulation to operate the numerical analysis. The numerical modelling provides us with different parameters like stress, strain and displacements in elastic and plastic behaviour.

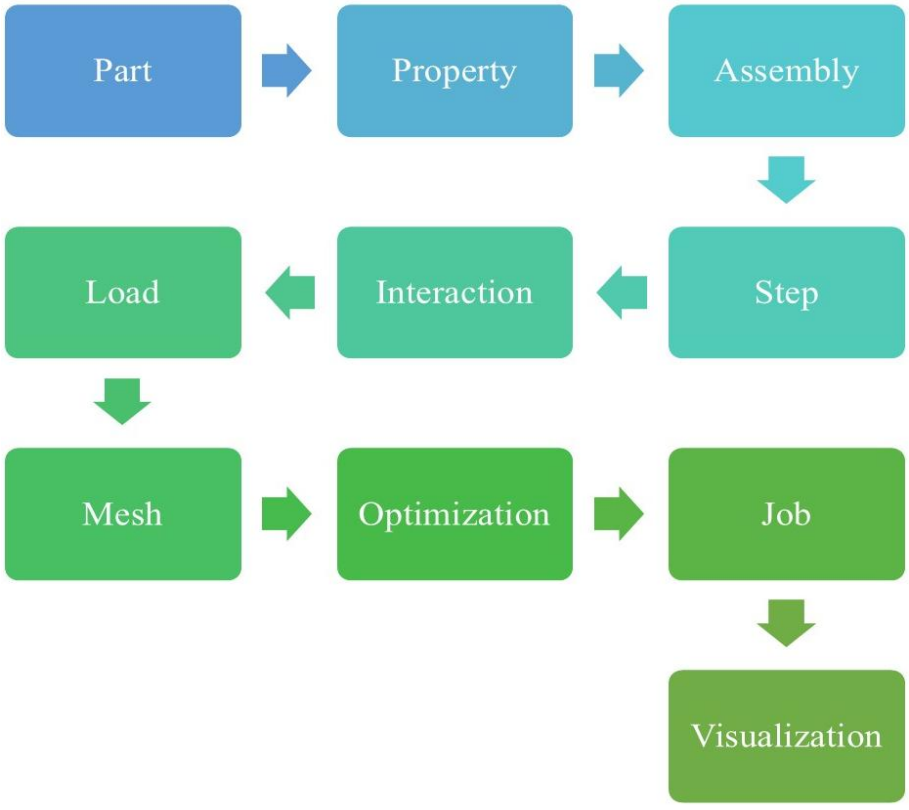

Figure 4**:** Flow chart for showing the step-by-step procedure for conducting the numerical analysis i.e., from initialization of the simulation to the visualization of the results

4.1. Conceptualization of damage and flow

The concept carried out in the numerical method is based strain circle which is based on Mohr's circle method for damage and flow in geomaterial subjected to vibratory loads. The strain circle is defined in terms of yielding strain and elastic strain. The strain circle is made with the help of dilation angle and flow ratio as shown in Fig. 5. The geomaterial sample is a loose sand, so the dilation angle is considered to be 2.5°.

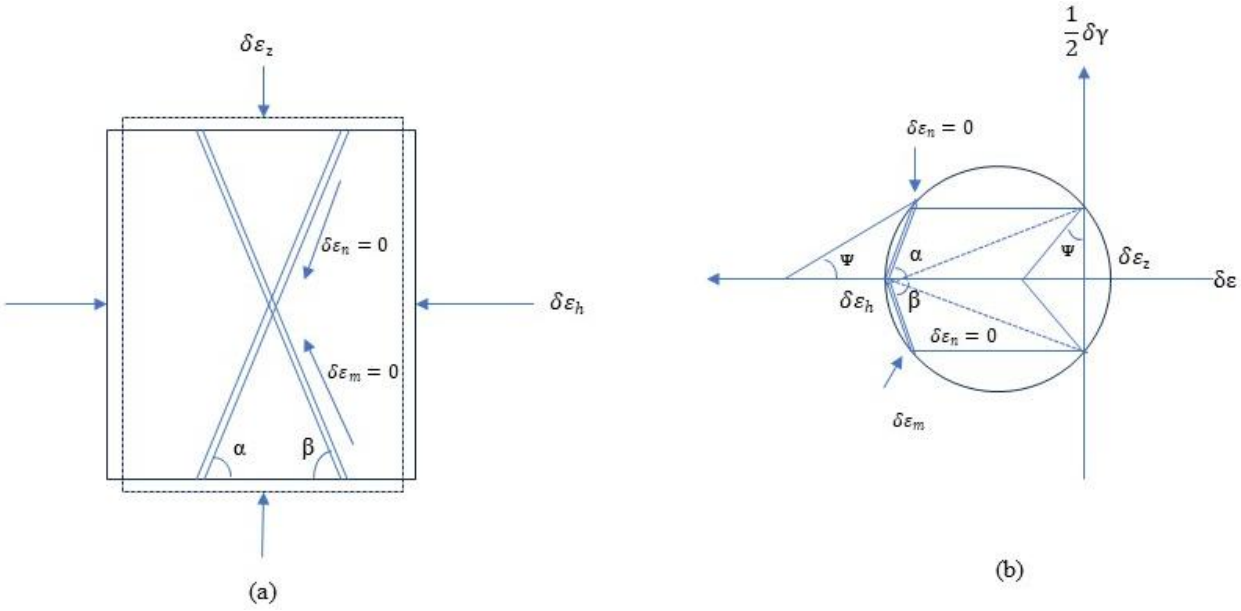

Figure 5: Graphical representation of (a) Angle of dilation where deformed plane under horizontal ($\delta\varepsilon_h$) and vertical strain ($\delta\varepsilon_z$) is shown with dotted line deforming the original plane and (b) zero extension line shown in strain circle constructed with the help of yielding (δ_γ) and elastic strain ($\delta\varepsilon$)

The planes showed by double lines on which the flow ratio occurs are at angle α and β as shown and from the geometry of the Fig. 5,

$$\alpha = \beta = 45° + \frac{1}{2}\phi_m \quad \text{.....(9)}$$

For the flow in geomaterial these correspond to the planes on which the most critical conditions occur and they should be the planes on which the failure will occur.

When the major and minor principal strains have opposite signs the origin of the axes is inside the strain circle, as shown in Fig. 5(b). there are two planes, shown by the broken lines in Fig. 5(b), across which the normal strains are zero, and so there are two directions, as shown in Fig. 5(a). these planes are defined by an angle of dilation Ψ.

$$tan\Psi = -\frac{\delta\varepsilon_v}{\delta\gamma} \quad \text{.....(10)}$$

Fig. 6 is a graphical representation of volumetric strain versus horizontal strain in which due to dilation it is shown that first vertical strain decreases then increases with increase in axial strain. Volumetric strain is denoted by ε_v and axial strain is denoted by ε_h.

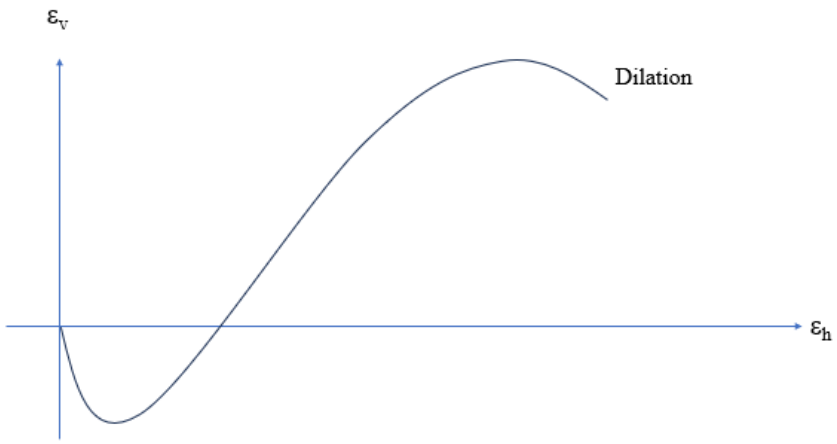

Figure 6: Graphical representation of volumetric strain versus axial strain with influence of dilation

This behaviour of hysteresis curve and stress-strain characteristic can be explained by Fig. 7 in which Fig. 7(a) shows a normal set of geomaterial in which load is about to be applied. Fig. 7(b) shows the after effect of load applied in which geomaterial particles are contracted among themselves and get displaced from the original position. It is hypothesized that when the stress is increasing, strain will increase but after some time it will decrease. It is so because firstly the geomaterial particles were in loose state but after applying the load, they will contract and

after certain they will start to give resisting force as they are completely packed and get the strength to reflect back.

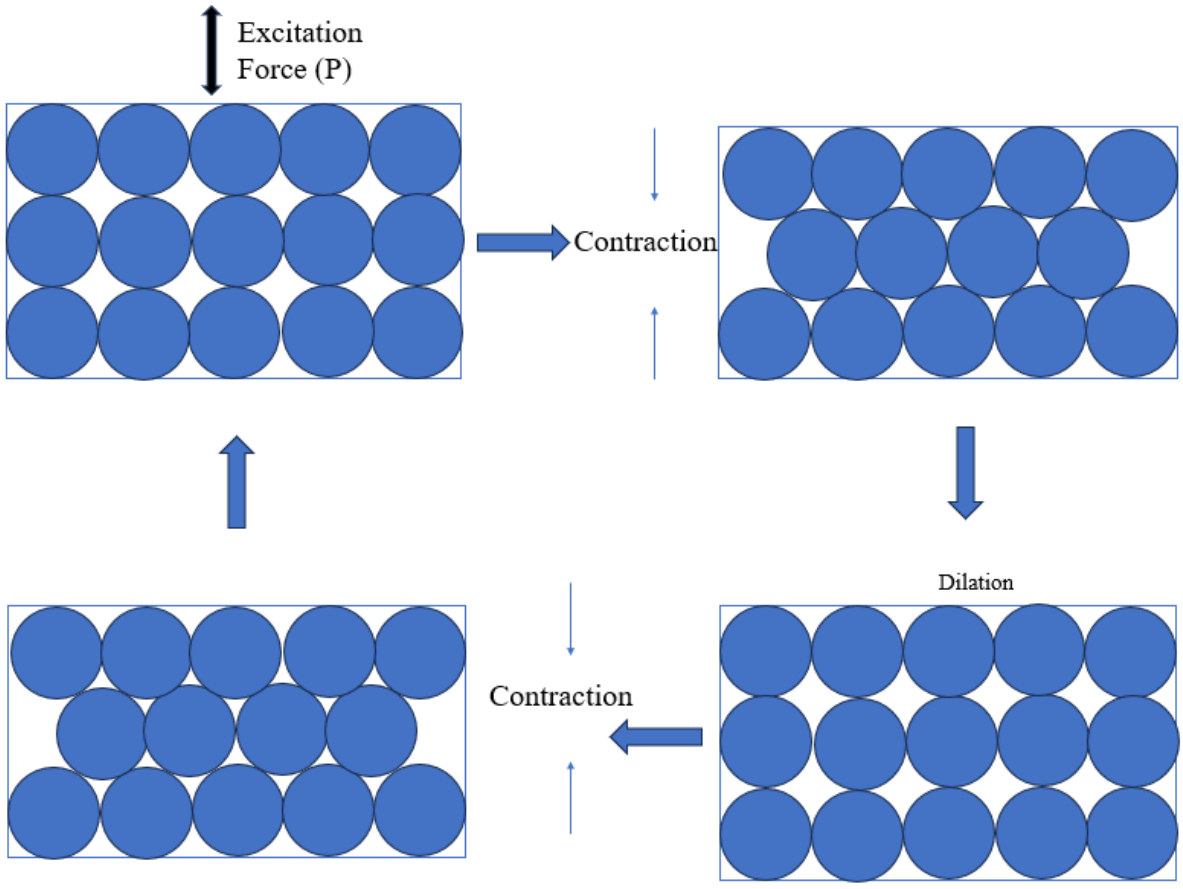

Figure 7: Contraction of geomaterial particles after applying load (a) Before application of load (b) After application of load

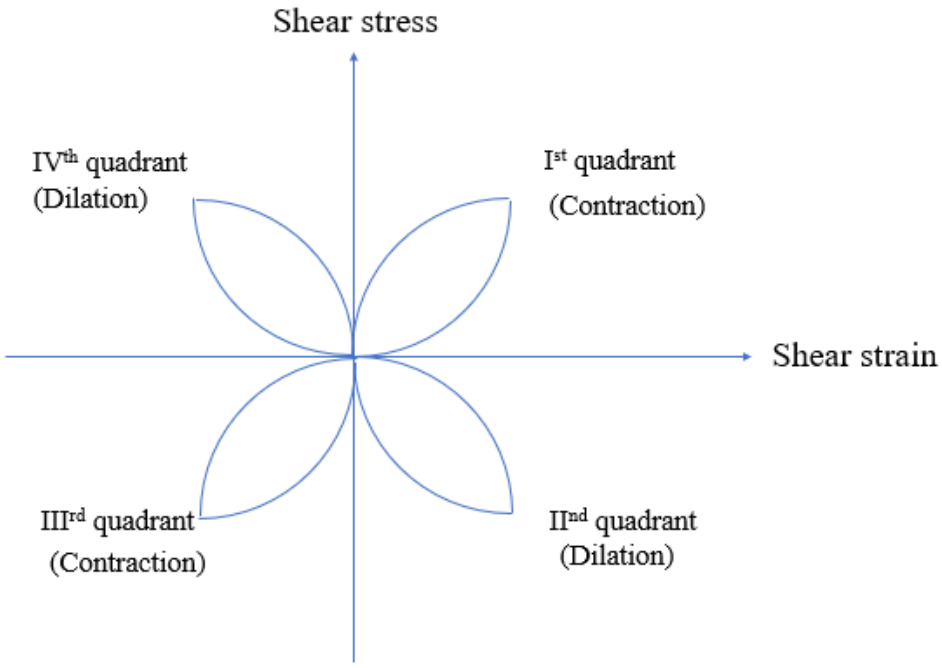

Figure 8: Evolution of stress-strain characteristics hypothesized from Ist quadrant (dilation) to IVth (tension) then to IInd (tension) and then to IIIrd (dilation) quadrant with certain range of scale (femtoscale to kiloscale)

A hypothesis is carried out that stress-strain characteristics should come in certain quadrant after the application of load. Fig. 8 is a graphical representation of the hysteresis curve which shows that after applying the load the curve starting from zero moves towards first quadrant the to fourth quadrant then towards second quadrant and lastly to the third quadrant. Due to loading and unloading of the load a cycle is created in which these steps are again and again repeating and a flower like pattern should be seen after the results are obtained.

4.2. Foundation concept for damage and flow in geomaterial subjected to vibratory loads

The geomaterial supported by the paving layers is observed to be in continuous contact with the boundaries of the MS steel tank where elastic analysis is carried out. At the bottom surface of the pavement layer particular deformation occurs in geomaterial. In this study, it is observed that shear stress is linearly dependent on normal stress. So, a technique is adopted for the

evaluation of damage and flow in geomaterial subjected to vibratory loads, which can be obtained by the assumptions mentioned below:

a) In the yielding surface, the behaviour of geomaterial is elastic. The plastic yielding surface assumes the initial behaviour to be nonlinear hardening.
b) A stress-strain law is followed by flow controlled geomaterial as a function of I_1, J_2 and J_3 and has beginning of nonlinearity at $\varepsilon^p_{ij}>0$.
c) If $f=0$, then shear norm for flow in geomaterial intersect the yields surface as smooth which makes it a special case.
d) Plastic stress-strain chain rule is followed by flow in geomaterial given as $(\delta f/\sigma_{ij})\ \delta\sigma_{ij} >0$.
e) In the deviatoric stress plane the shape of smooth flow in geomaterial is elliptical and in meridional stress plane it is hyperbolic with eccentricity.

After assuming these criteria, the yield function can be represented as:

$f=\sigma_e-\sigma_y$.....(11)

if $f<0$ (elastic zone)

or $f=0$ (plastic zone)

and $\frac{\partial f}{\partial \sigma_{ij}} \partial_{ij} > 0$

where, $\sigma_e = \sqrt{\frac{3}{2}\sigma:\sigma}$

$\sigma_{y=} f(p)$ expressed as

$\sigma_y = f(p) = \sigma_{y0} + H\varepsilon^p,\ (\varepsilon^p = p + \Delta p)$.....(12)

in this study, H is taken as a function of friction angle, dilation angle, frequency and load.

After the load applied, the total strain (ε_{ij}) is varied such that $\partial\varepsilon\, p_{ij} \neq 0$, the stress points support the yield surface which is ensured by the consistency conditions expressed as

$$\partial f = \left(\frac{\partial f}{\partial_{ij}}\right)\partial\sigma_{ij} + \left(\frac{\partial f}{\partial\varepsilon_{ij}}\right)\partial\varepsilon^{p}{}_{ij} = 0 \quad (13)$$

The increment for plastic strain, ($\varepsilon^{p}{}_{ij}$) direction is given as

$$d\varepsilon = \partial\lambda\partial g/\partial\sigma_{ij} \quad (14)$$

The modified yield onset for any flow in geomaterial would be first stress invariant function. The yield criteria for the flow in geomaterial if the stress state lies on the single yield function can be given as:

$$f = \sigma_3 - \sigma_1 + (\sigma_3 + \sigma_1)\sin\phi \quad (15)$$

the dilation angle ϕ_d gives plastic potential given as,

$$g = \sigma_3 - \sigma_1 + (\sigma_3 + \sigma_1)\sin\phi_d \quad (16)$$

The flow in geomaterials is assumed to follow the strain circle failure criteria as mentioned in Fig. 5.

CHAPTER 5

MODEL TESTING

The schematic diagram of model assembly shown in Fig. 9 demonstrates a dynamic test apparatus intended to study the response of geogrid-reinforced geomaterial under vibratory load conditions. A mild steel (MS) tank containing geogrid-reinforced geomaterial is at the center of the system. Piezoelectric (PZT) sensors are mounted strategically on the side walls of the tank to pick up stress waves and dynamic response within the material. Mounted on the surface of the geomaterial is a dynamic actuating vibrator, which acts as the source of mechanical excitation. This is driven and controlled by a signal generator, which supplies electrical signals to cause dynamic loading of known frequencies and amplitudes.

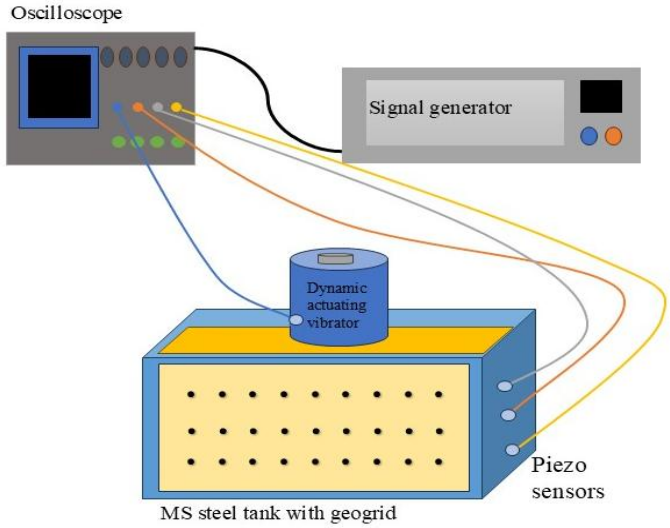

Figure 9: Diagrammatic representation of the model testing consisting of digital storage oscilloscope, power amplifier cum signal generator, dynamic actuating unit, MS steel tank with and without geogrid reinforced geomaterial, and piezo sensors

The pictorial sketch of the model assembly consisting of dynamic actuating vibrator, MS steel tank, geogrid, and geomaterial is shown in Fig. 10. The voltage response with time is obtained for the selected set of frequencies, namely, 5-30 Hz with an increment of 5 Hz.

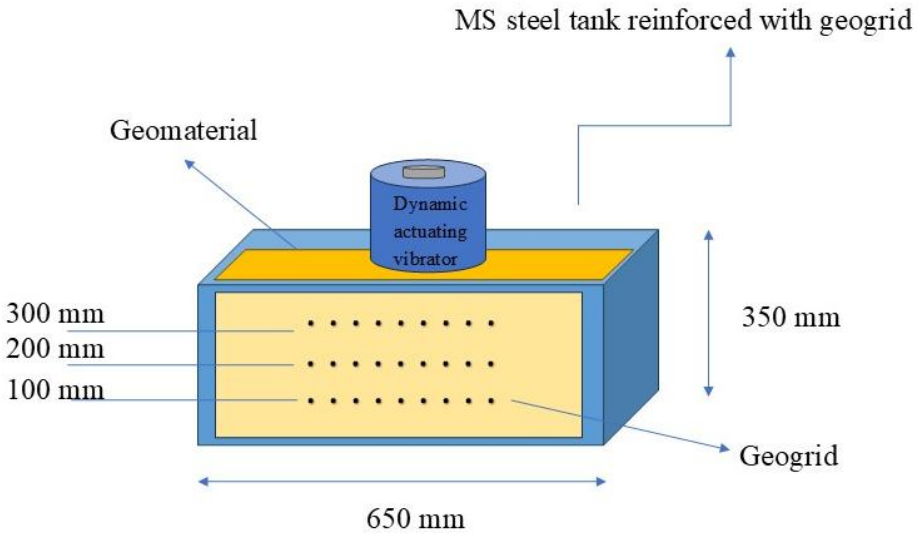

Figure 10: Pictorial representation of the placement of the geogrid layer in the MS steel tank at different depths

Table III: Properties of geogrid obtained from the manufacturer

S.no.	Geogrid	Value	Units
1.	Aperture size	30×30	mm
2.	Ultimate tensile strength	38.1	kN/m^2
3.	Yield strain	16.7	%
4.	Secant modulus at 2% strain	588	kN/m^2
5.	Mass per unit area	5.20	kN/m^2

Table III briefly describes the properties of geogrid which is used as a reinforcement material made up of geosynthetic polymer. The piezo sensors that sense the induced vibration by creating electrical signals that are proportional to the stress or strain caused are connected to an oscilloscope. This oscilloscope records and presents the actual time data, and it is possible to analyze wave propagation properties, stiffness variation, and damping behavior of the reinforced geomaterial. The synchronized interface among the signal generator, actuator, piezo

sensors, and oscilloscope creates a complete test system with the ability to simulate dynamic field conditions. This configuration is especially beneficial in studying the performance gains provided by geogrid reinforcement in unpaved roads or other geotechnical structures under vibrational loading.

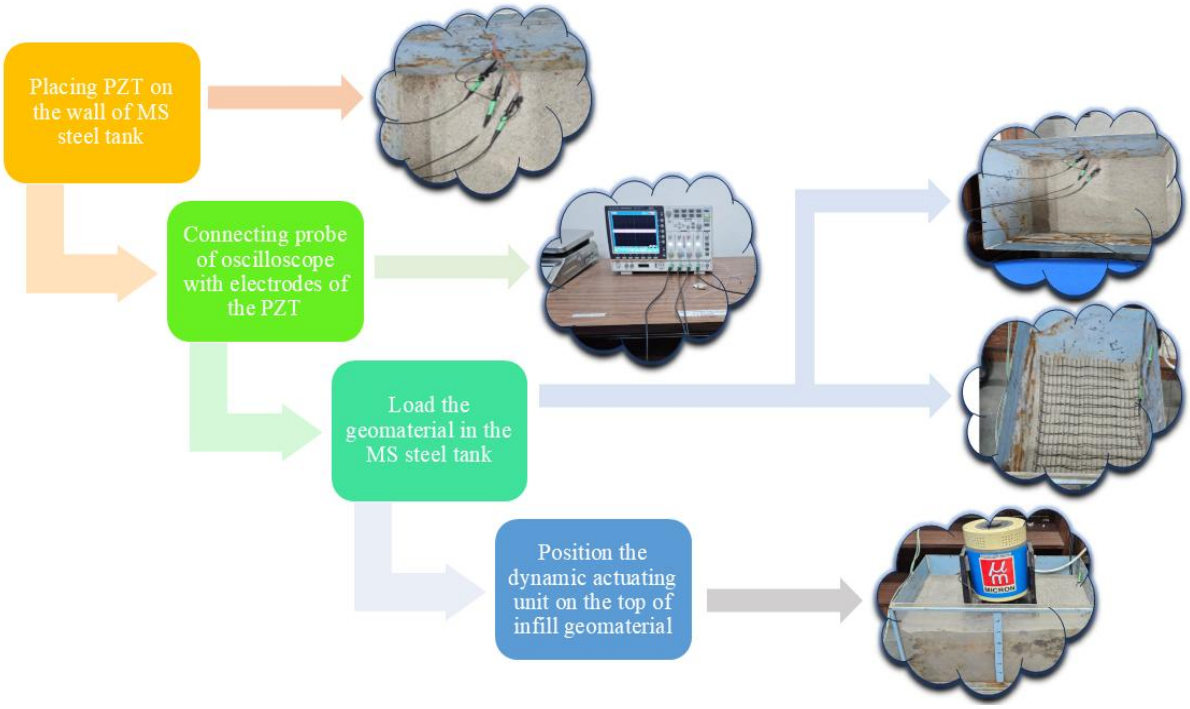

Figure 11**:** Pictorial representation of the testing procedure carried out in model analysis where (a) piezo sensors are attached to the MS steel tank at different depths, (b) connecting the probes of oscilloscope with the electrodes of the PZT for analyzing the output, (c) loading of geomaterial in the MS steel tank with geogrid sheets, and (d) position the dynamic actuating unit on the top of infill geomaterial

Fig. 11 briefly describes a step-by-step experimental arrangement for dynamic testing of geomaterials with piezoelectric (PZT) patches and an oscilloscope inside a mild steel (MS) tank. The procedure starts with installing PZT sensors on the inner wall of the MS steel tank, which are used to observe wave propagation and dynamic response. These PZTs are subsequently joined to an oscilloscope by means of probes coupled to their electrodes so that they can pick up real-time voltage signals as developed during tests. After having the sensors deployed and securely joined, the desired geomaterial is loaded slowly into the steel tank. A

dynamic actuating unit is next placed on top of the infilled geomaterial. This unit provides cyclic or vibration loads that model traffic vibrations, thus triggering wave propagation through the material. The oscilloscope records signals passed through the geomaterial with the ability to analyze wave development and damping properties. The experimental arrangement, involving strategic placement of PZTs and precise instrumentation, is effective in monitoring dynamic interaction between actuating forces and the geomaterial, yielding significant information regarding the mechanical response of soils under dynamic loading. The arrangement is best suited for studying the performance of unpaved road bases or soil systems under vibration.

5.1. Dynamic voltage response

The voltage generated by the dynamic actuating vibrator is of harmonic nature; Hence, it can be presented as:

$$V_e = V_0 \cos \omega t \quad (17)$$

Solution of this equation could be obtained as follows:

$$V(t) = V(t)_{CF} + V(t)_{PI} \quad (18)$$

Here, subscripted CF denotes solution in terms of complementary function, and PI denotes solution in terms of a particular integral. In solving non-homogeneous differential equations, the method of undetermined coefficients or variation of parameters is often used. Both methods require finding a particular solution to the non-homogeneous equation. While using the method of undetermined coefficients, a particular form for the solution is assumed based on the form of the non-homogeneous term. To avoid redundancy, any term in the assumed solution that already exists in the complementary function is excluded (the solution to the corresponding homogeneous equation). The complementary function already accounts for the homogeneous part of the solution, and if those terms appear again in the particular solution, it will lead to overcounting. So, setting the complementary function equal to zero avoids the duplicacy of any terms in the particular solution.

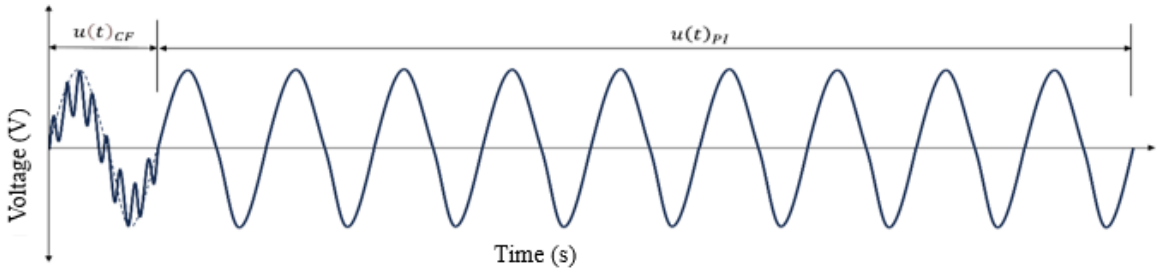

Figure 12: Diagrammatic conceptualization of the complementary function and particular integral assumed in the present research

This approach helps streamline the process of finding a particular solution and ensures that there are no redundancies in the solution. Hence, to find out CF, it is assumed that the system of forces would behave the same as that for underdamped free vibration. It is assumed from the basic understanding of the mechanics, that the CF is an exponential decay function, and the particular integral is a harmonic function. Conceptually, it can be understood by the Fig. 12 as depicted below:

CHAPTER 6

CALIFORNIA BEARING RATIO TEST

In the experimental setup as shown in Fig. 13, geogrid layers are strategically placed within the mould to assess its impact on the strength characteristics of the material under-soaked conditions. The mould was then submerged in water for a duration of 96 hours with geogrid layers reinforced in geomaterial. The soaking period is intended to simulate conditions that may affect the performance of geogrid, particularly strength retention under saturated conditions.

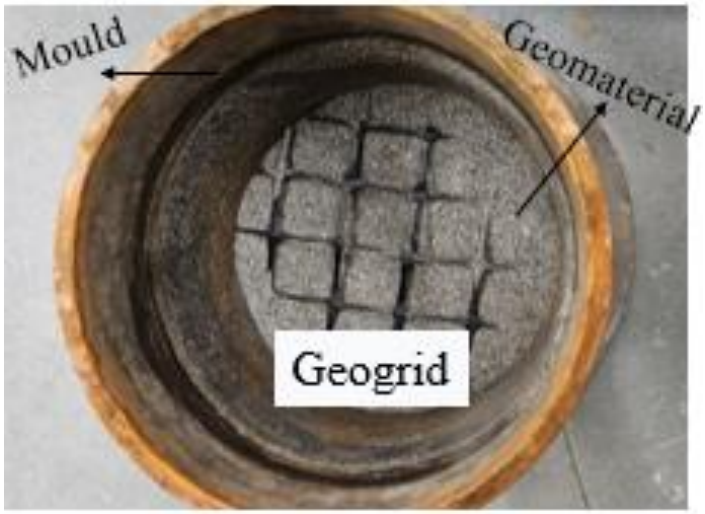

Figure 13: Pictorial representation of the geomaterial reinforced with geogrid placed inside CBR mould before soaking for 96 hours

The test is conducted under three distinct conditions as shown in Fig. 11, is categorized as follows:

a) Geogrid at h/2 depth,
b) Geogrid at h/3 depth, and
c) Geogrid at h/4 depth.

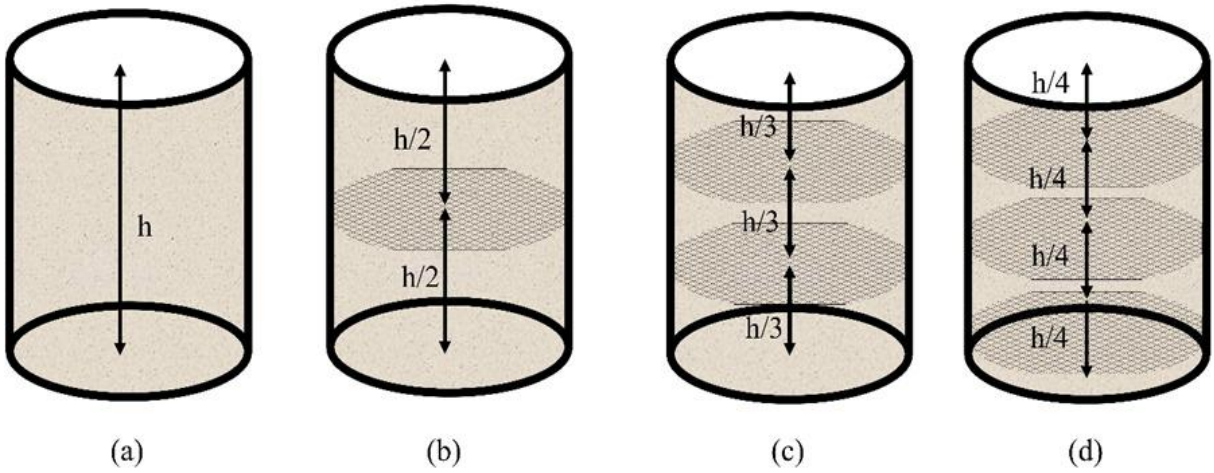

Figure 14**:** Pictorial representation of geomaterial reinforced with geogrid in CBR mould at varied height as (a) empty tank with height h, (b) at h/2 depth, (c) at h/3 depth, and (d) at h/4 depth

Fig. 14(a) shows pictorial representation of empty CBR mould with height h which is afterwards is filled with geomaterial and reinforced with geogrid at varied depth.

With the help of CBR test, certain parameters are calculated which includes penetration (mm), load intensity(kN/m^2), stiffness capacity, and penetration factor. The calculation is carried as mentioned below.

Stiffness capacity = k/k_{max}.....(19)

where, k is stiffness and k_{max} is maximum stiffness

and, $k = \frac{force\ applied}{displacement}$

$Penetration\ factor = \frac{obtained\ penetration}{(maximum\ penetration)}$.....(20)

CHAPTER 7

RESULTS AND DISCUSSION

7.1. Evaluation of damage and flow in geomaterial subjected to vibratory loads

The variation of load and friction angle have been considered to understand the evolution of damage and flow controlled geomaterial subjected to vibratory load. Fig. 15 shows the progressive flow damage in geomaterial subjected to vibratory load of varied input frequencies. The accumulating flow stress with strain accounting for damage has been recorded from femto ($\sim 10^{-15}$ m) to macroscopic (10^{3} m) scales. It has been observed that represents the evolvement of the stress versus strain makes a flower like structure which are the representation of multiple hysteresis curve in collected way under cyclic loading and unloading which was hypothesized in Fig. 6. Fig. 15(a), (b), (c), (d), (e), and (f) obtained values after hypothesis comes to be correct which ranges from (-5×10^{-14} to 5×10^{-14}), (-6×10^{-8} to 2×10^{-8}), (-6×10^{-3} to 8×10^{-3}), (-4 to 4), (-400 to 400), and (-1000 to 1000) respectively.

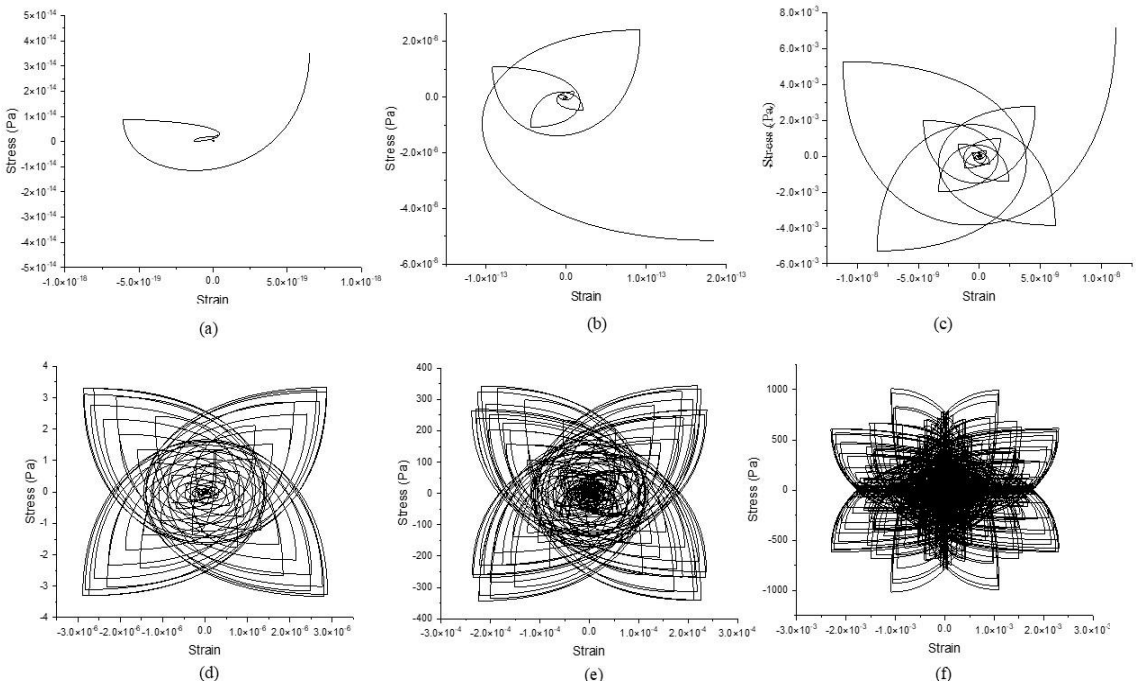

Figure 15: Graphical representation of cyclic stress versus strain evolution for the selected set of input parameters.

7.1.1. Influence of friction angle on stress-strain characteristics of confined geomaterial under vibratory loads

Fig. 16 shows the influence of friction angle on stress-strain characteristics of confined geomaterial under vibratory loads. The numerical modelling gives the simulation in flower like pattern which is happening because of the loading and unloading of the progressive flow damage in geomaterial subjected to vibratory load. As assumed in the methodology, at different friction angle the simulation provided from the numerical modelling the stress-strain should be in different types of scale. It is proved from Fig. 15 that the evolution assumed is giving the right nature of values. In Fig. 16 the friction angle is considered at different levels with the interval of five degrees. Fig. 16(a), (b), (c) and (d) represents the stress-strain graph of friction angle 25°, 30°, 35° and 40° respectively. It is observed that with more friction angle stress-strain characteristics decreases which is a normal behaviour for geomaterial to react.

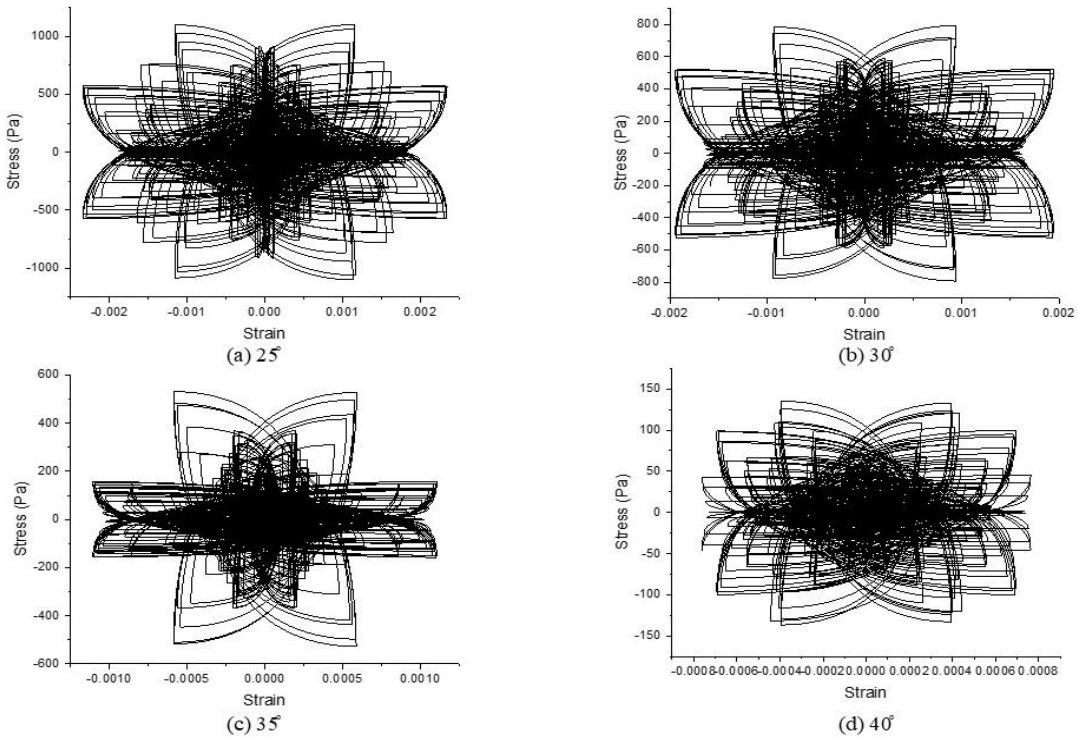

Figure 16: Graphical representation of stress versus strain rosette at varied friction angle ranging from 25° to 40°

7.1.2. Impact of load on stress-strain characteristics of confined geomaterial subjected to moving loads

Fig. 17 describes the impact of load on stress-strain characteristics of confined geomaterial subjected to moving loads. Fig. 17(a), (b), (c) and (d) defines the loads as 2.5, 5, 7.5 and 10 kN respectively. The flower like pattern explains the behaviour of stress and strain in all the four directions which shows that the effect of load is very much different from the friction angle which is happening due to volumetric shift and effect of dilatancy. The increase in load shows the decrease in stress-strain characteristics in geomaterial subjected to vibratory load.

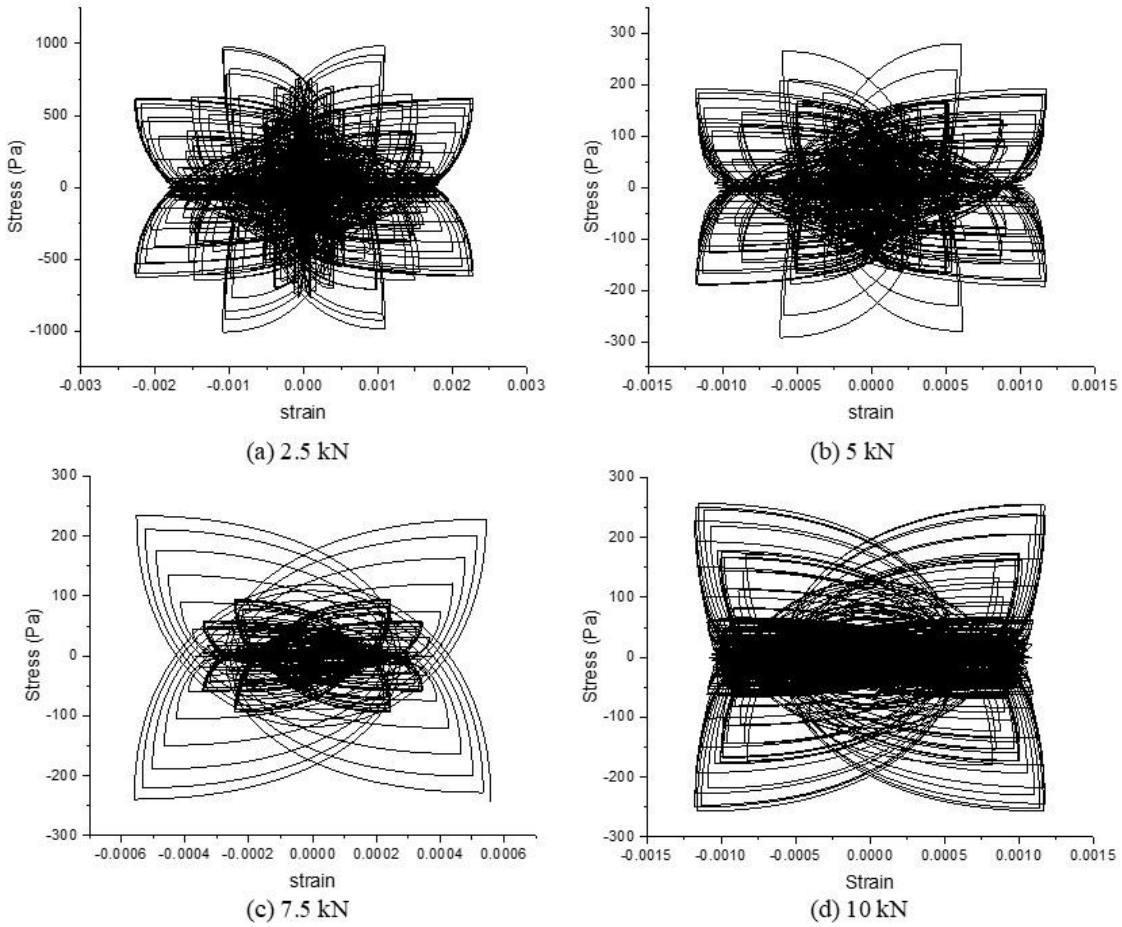

Figure 17: Graphical representation of stress versus strain rosette at varied loads ranging from 2.5 to 10 kN

7.1.3. Stress-strain characteristics in terms of shear modulus (G) and the role of friction angle and load on damage and flow

Fig. 18 shows the comparison generated with different friction angle and load in terms of shear modulus. It is calculated from the stress-strain obtained from the damage and flow evaluation of reinforced geomaterials subjected to vibratory loads. At horizontal axis, shear modulus is taken in decreasing order, at primary vertical axis different friction angle is taken and at secondary vertical axis load is taken. The graph depicts that by increasing the friction angle gradual decrease in the shear modulus is seen and while load increases sudden decrease of shear modulus is observed. This behaviour of geomaterial describes that more friction angle and load reduce the shear strength of the geomaterial which generally indicates that geomaterial is more resistant to shear deformation, but it does not directly dictate the shear strength, which is the maximum shear stress a geomaterial can withstand before the failure.

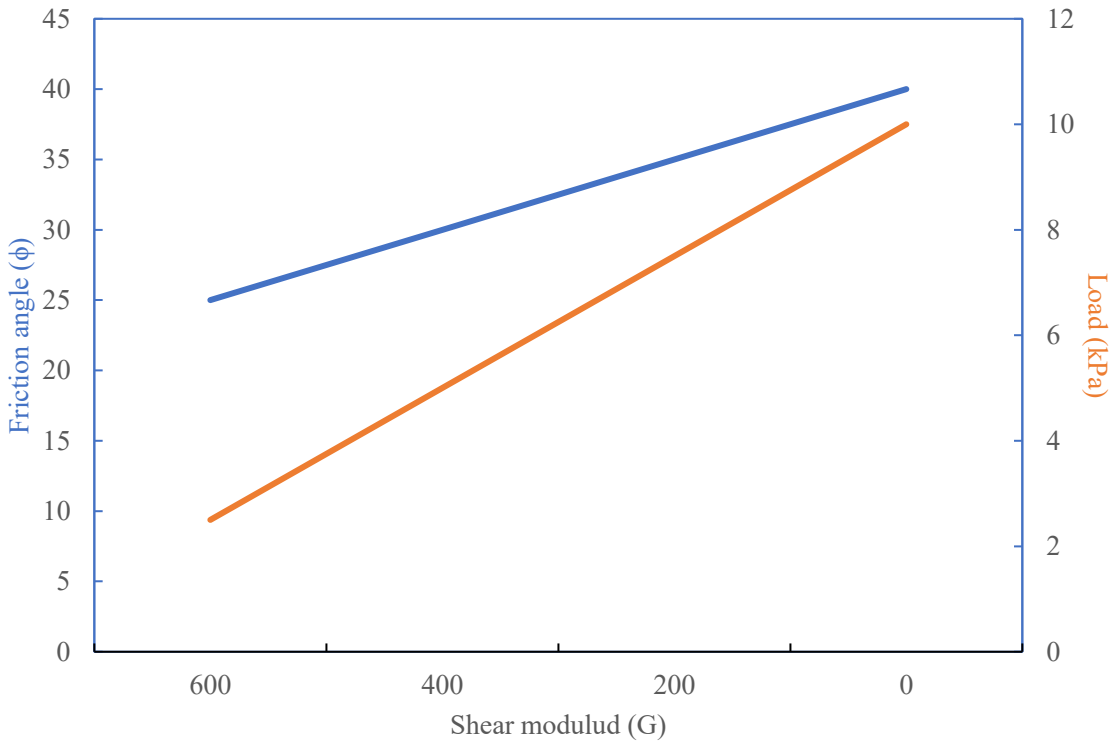

Figure 18: Graphical representation of shear modulus with friction angle and load for varied friction angle and load

7.2. Effect of geogrid reinforcement on cohesionless subgrade

Fig. 19 shows a comparative analysis of voltage response with time for selected states of soil reinforcement with geogrid of varying embedment depths (100 mm, 200 mm, 300 mm, and dynamic actuating vibrator, DAV mounted on top surface of geo material). For a lower frequency input from DAV, a significant waveform oscillation was observed. The unreinforced case (normal) at shallow embedment (100 mm and 200 mm) shows that the voltage signals have larger amplitudes and more random oscillations, suggesting higher system instability and sensitivity to external vibrations. The reinforcement of geogrid in geomaterial is seen to dampen the oscillations, suggesting damping function to mitigate the dynamic responses, particularly at deeper embedment such as 30 cm. The geogrid embedded at 300 mm shows that the signals are more stable and of lower amplitude during the time interval compared to the unreinforced sections. The results indicate that geogrid reinforcement significantly improves stability and reduces dynamic voltage responses in geomaterial, especially at deeper embedment levels. The most apparent trend in all the graphs is that greater embedment levels and the use of geogrid always result in reduced voltage amplitudes and damped signals, which confirms the virtue of capturing dynamic response.

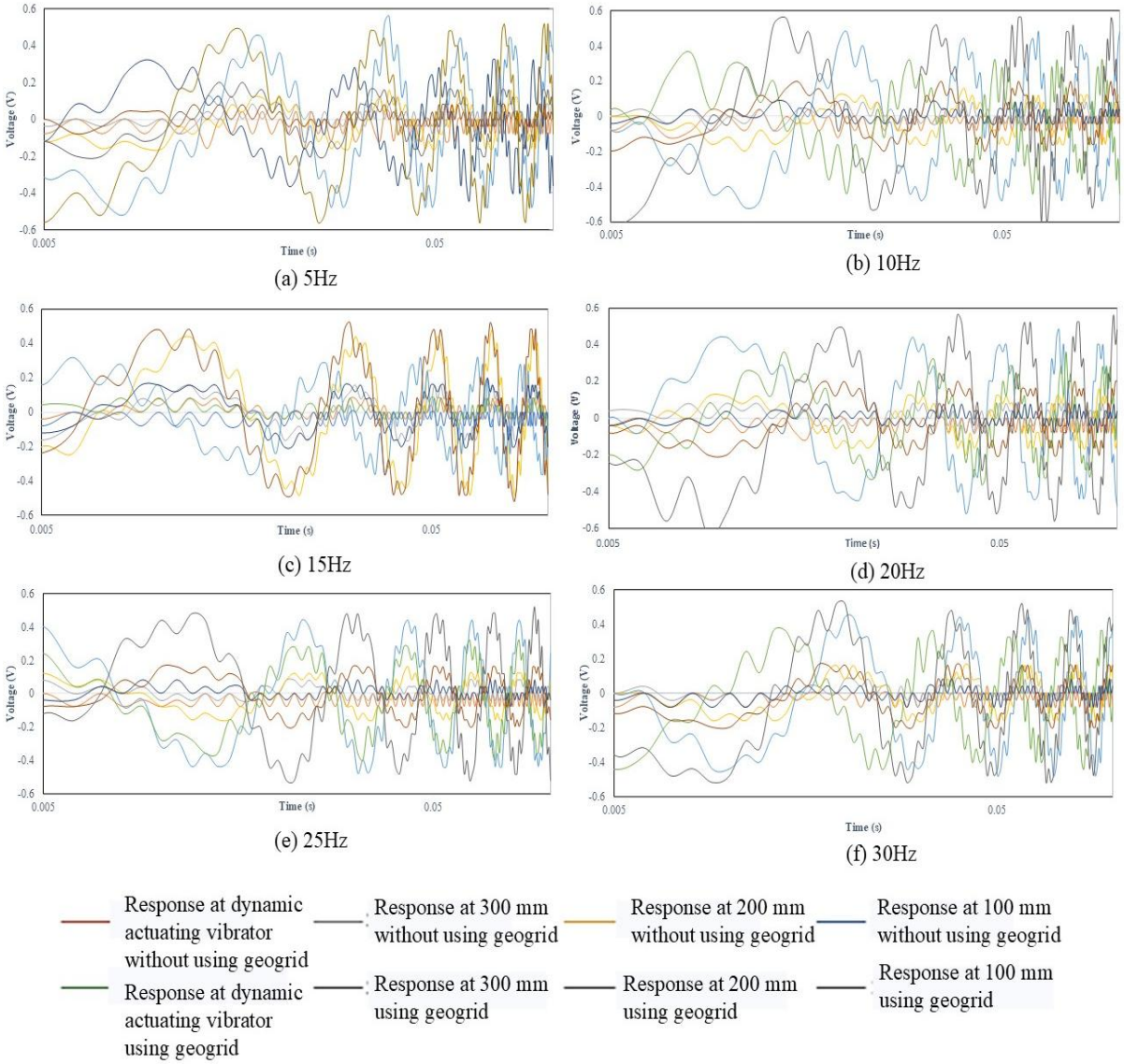

Figure 19: Graphical representation of voltage versus time at varied frequencies from 5 to 30 Hz obtained using model analysis with piezo sensors

7.3. Variation of stiffness capacity with penetration factor

Fig. 20 shows the variation of stiffness capacity (k/ k_{max}) with the penetration factor for varied depths of geogrid reinforcement in the geomaterial. The results of the present work and jute reinforcement have been compared with reinforced sections using geogrid and jute at different depths (Kumar et al., 2023). The results show the effectiveness of reinforcement in resisting stiffness loss and the influence of reinforcement depth on performance.

The geogrid reinforcement controls the loss of stiffness capacity as penetration increases. Geogrid at h/2 depth shows a gradual decline in stiffness capacity, indicating a better performance than the unreinforced section. Similarly, the geogrid at h/3 and h/4 depths shows improved performance, with h/4 depth being the section with the highest stiffness capacity. The variation of stiffness capacity suggests that placing geogrid reinforcement at a greater number of levels (h/3 and h/4) results in better load distribution and improved resistance to penetration-induced stiffness loss.

Jute at h/2 depth shows a sharp decline in stiffness, performing slightly better than the unreinforced section. Jute at h/3 depths performs better than h/2 placement but does not maintain stiffness as well as the geogrid counterparts. Jute at h/4 depths retains the highest stiffness capacity among the jute-reinforced sections, reinforcing the trend that deeper reinforcement placement is more effective. Compared to geogrid, jute reinforcement exhibits a faster reduction in stiffness capacity, indicating that natural fibers may degrade more quickly or provide less overall structural resistance.

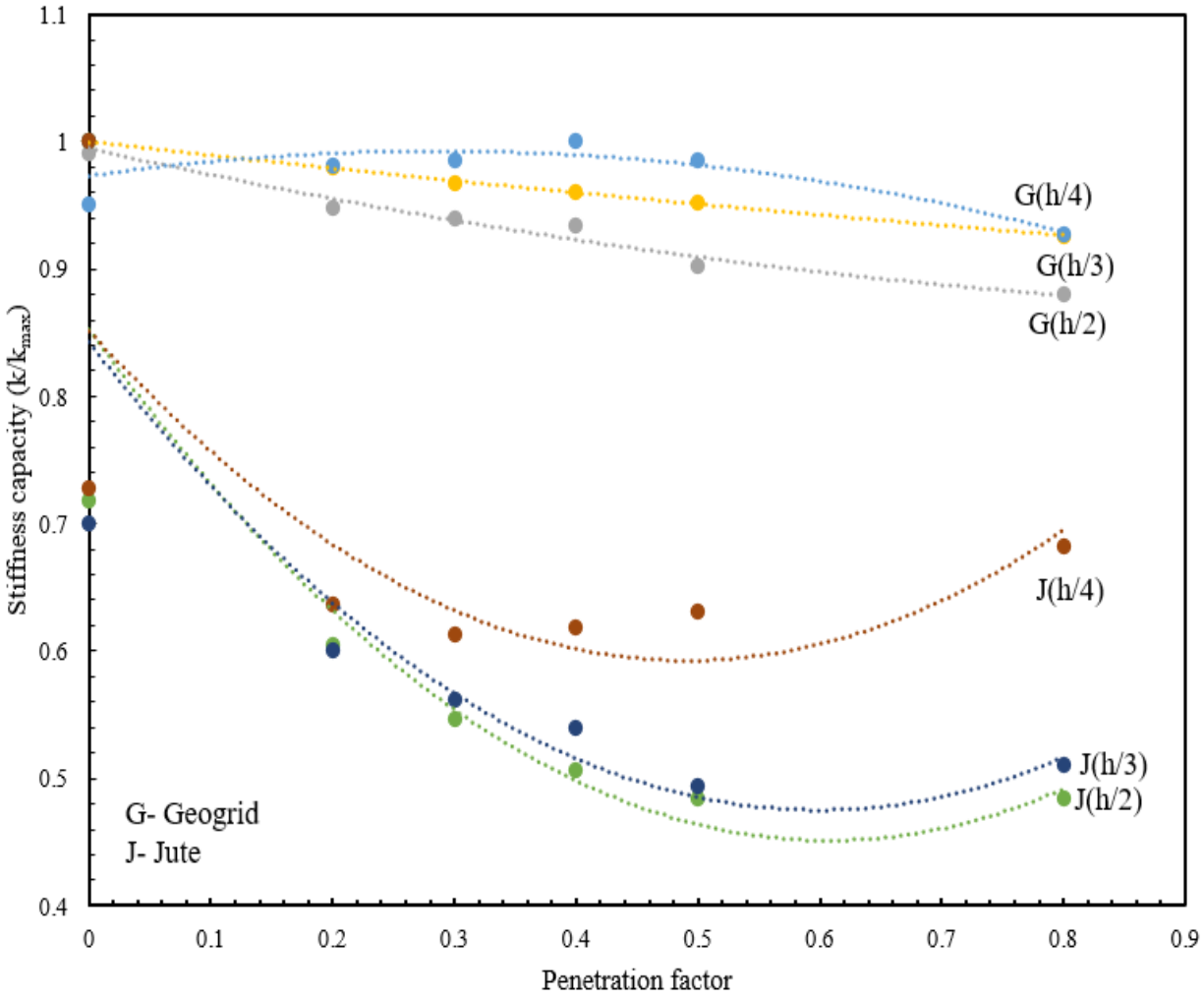

Figure 20: Comparison of geogrid (present work) and jute reinforcement for stiffness capacity and penetration factor (Kumar et al., 2023) and the reinforcement (in both the cases) varied at h/2, h/3, and h/4 depth of the MS steel tank

7.4. Variation of penetration with load intensity

Fig. 21 shows the relationship between penetration (mm) and load intensity (kN/m²) for different reinforcement conditions. The dataset includes results from both the geogrid and jute reinforcement, comparing the performance of reinforced sections using geogrid and jute placed at varied depth.

Geogrid-reinforced sections show the lowest penetration values, demonstrating their effectiveness in resisting deformation. Geogrid at h/4 depth shows lowest penetration values for the selected set of load intensities. Similarly, geogrid at h/3 depth and h/2 depth show significant improvement. The results indicate that placing geogrid at a greater number of depths enhances stability, as the reinforcement is better positioned to distribute loads and resist geomaterial displacement.

It has been observed from the findings that, the geogrid reinforcement performs better than reinforced sections as well as the jute-reinforced sections. Jute at h/4 depth shows the best performance among the jute-reinforced sections, followed by h/3 depth and h/2 depth. However, compared to geogrid reinforcement at the same depth, jute-reinforced sections exhibit higher penetration, suggesting that geogrid is structurally stronger and more effective in controlling deformation. The sharp increase in penetration beyond 5 kN/m² in jute-reinforced sections indicates that jute may lose effectiveness under higher loads, possibly due to material deformation or biodegradability.

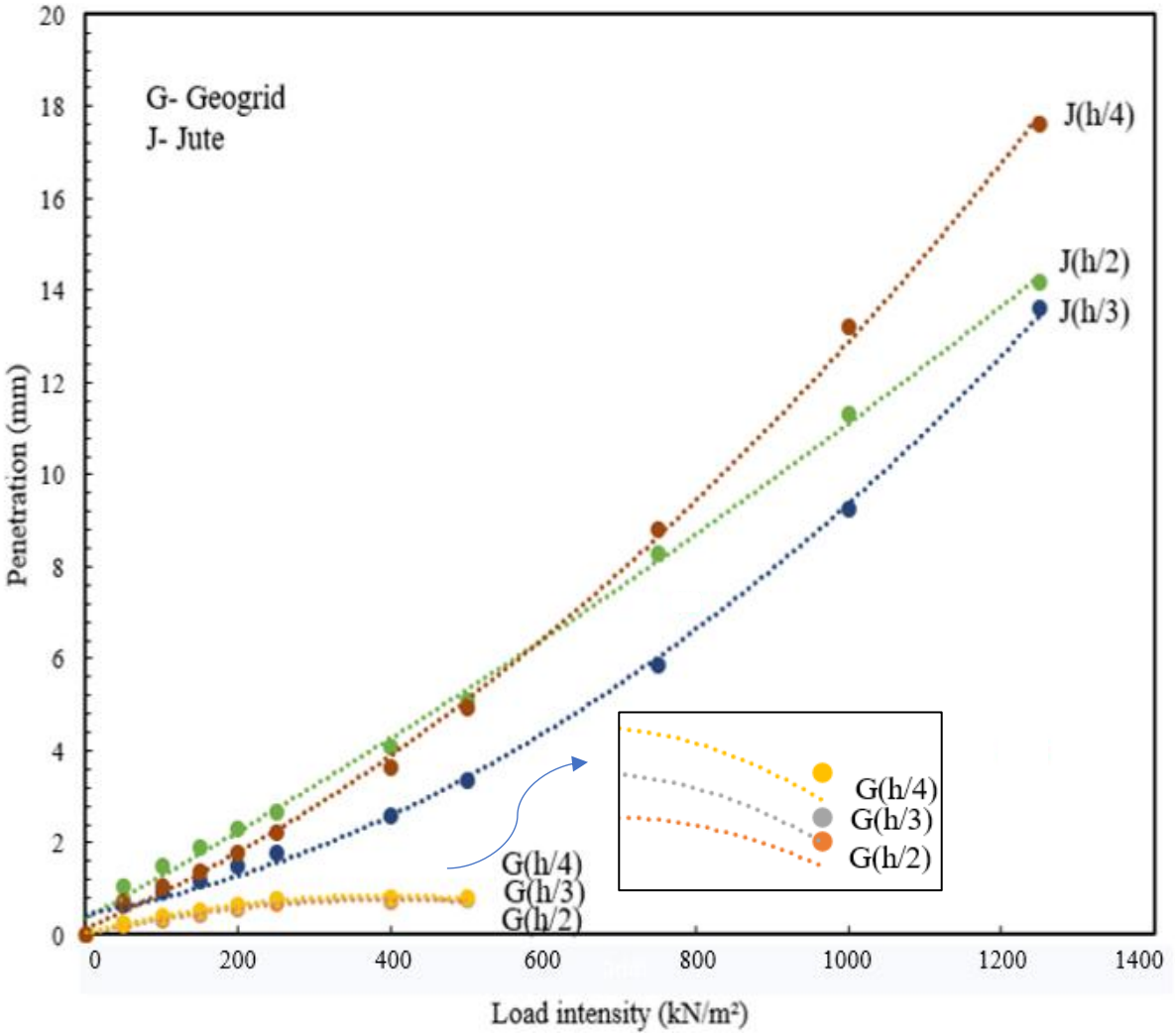

Figure 21: Comparison between geogrid (present work) and jute in terms of penetration and load intensity (Kumar et al., 2023) the reinforcement (in both the cases) varied at h/2, h/3, and h/4 depth of the MS steel tank

CHAPTER 5

CONCLUSION AND FUTURE SCOPE

In the presented research work, damage in terms of stiffness capacity, penetration factor, damping and flow control has been evaluated for confined geomaterial subjected to vibratory loads. Based on the results and discussion presented earlier, the following conclusions has been drawn:

1. The shear modulus is obtained from stress-strain characteristics which shows that lesser values of friction angle and load gives more shear strength to the geomaterial as the stress increases strain increases as described in Table IV.
2. The variation of voltage with time has been obtained for confined geogrid reinforced sections of geomaterial for the selected set of input frequencies (5-30 Hz). The increase in the number of geogrids layers increase the stability, improves damping and strength.
3. It has been observed that increase in the friction angle (25-40) and load (2500-10000 N) reduces the stress a compounded transitioning of the stress hysteresis has been observed for the selected set of parameters.
4. The geogrid reinforcement significantly improves stiffness capacity than the jute as observed from the stiffness capacity and load-penetration factor. The observations indicates that more stiffness capacity provides better performance to the confined geomaterial at similar penetration factor. Table V shows the magnitude of geogrid for the graphical representation of Fig. 18 and 19 in which stiffness capacity and penetration are carried out at same load intensity respectively.
5. The reduction of penetration with load gives better stability and strength to the confined reinforced state of geomaterial. Jute is an ecofriendly method to reinforce the substructure however it provides less stability than geogrid reinforcement.

The outcomes of the presented research can effectively be used by field engineers and practitioners to evaluate the behaviour of confined geomaterial under dynamic conditions.

The presented research is believed to be a first of its kind study and is likely to open a new field of enquiry for confined geomaterial dynamics.

Table IV: Evaluation of damage and flow in reinforced geomaterial subjected to vibratory loads

Effect of shear modulus on damage and flow of geomaterial				Stiffness capacity and penetration obtained at constant load intensity		
Condition	Shear modulus of geomaterial	Flow	Damage (%)	Geogrid at varied depth	Stiffness capacity (k/k_{max})	Penetration (mm)
Small strains (10^{-6} to 10^{-4})	High (200-1000 kN/m^2)	No flow	0	At h/2	0.92	0.75
Medium to large strains (10^{-4} to 10^{-2})	Moderate (25-200 kN/m^2)	Onset of yielding	1-20	At h/3	0.94	0.77
Post yielding strain (10^{-2} to 10^{3})	Low (0-25 kN/m^2)	Flow of geomaterial	20-50	At h/4	0.95	0.81

References

[1] Bajaj, M., & Padmanabhan, G. (2022). Experimental study on the factors influencing the performance of geogrid encased granular pile anchor installed in cohesionless soils. International Journal of Geosynthetics and Ground Engineering, 8(3), 39.

[2] Basas, V. G., Pantazopoulos, I. A., & Atmatzidis, D. K. (2020). Torsional and flexural resonant column testing of grouted sands. Soil Dynamics and Earthquake Engineering, 139, 106360.

[3] Fernández-Lavín, A., Ovando-Shelley, E., & Chamorro-Zurita, C. (2024). Damping ratio on lacustrine soils using the wavelet transform. Soil Dynamics and Earthquake Engineering, 180, 108583.

[4] Gao, J., Yang, Y., Bian, X., & Zhu, G. (2024). Study on dynamic shear properties of sulfate saline soil-geotextile interface with different salt content. Soil Dynamics and Earthquake Engineering, 183, 108807.

[5] Heiland, T., Aji, H. D., Wuttke, F., Stempniewski, L., & Stark, A. (2023). Influence of soil-structure interaction on the dynamic characteristics of railroad frame bridges. Soil Dynamics and Earthquake Engineering, 167, 107800.

[6] Kirtimayee, B., & Samadhiya, N. K. (2022). Performance of loosely skirted shallow foundation resting on reinforced sand under vertical loading. International Journal of Geosynthetics and Ground Engineering, 8(1), 17.

[7] Kumar, P., Kumar, Y., & Trivedi, A. (2023). Influence of Jute Reinforcement on the Stiffness Capacity of Cohesionless Pavement Geomaterials. In International Conference on Interdisciplinary Approaches in Civil Engineering for Sustainable Development (379-390). Singapore: Springer Nature Singapore.

[8] Mei, X., Sheng, Q., Cui, Z., Zhang, M., & Dias, D. (2023). Experimental investigation on the mechanical and damping properties of rubber-sand-concrete prepared with recycled waste tires for aseismic isolation layer. Soil Dynamics and Earthquake Engineering, 165, 107718.

[9] Peellage, W. H., Fatahi, B., & Rasekh, H. (2022). Experimental investigation for vibration characteristics of jointed rocks using cyclic triaxial tests. Soil Dynamics and Earthquake Engineering, 160, 107377

[10] Pires, A. C., & Palmeira, E. M. (2021). The influence of geosynthetic reinforcement on the mechanical behaviour of soil-pipe systems. Geotextiles and Geomembranes, 49(5), 1117-1128.

[11] Prasad, P. S., & Ramana, G. V. (2016). Feasibility study of copper slag as a structural fill in reinforced soil structures. Geotextiles and Geomembranes, 44(4), 623-640.

[12] Shafiee, A., Fathipour, H., Payan, M., Jalili, J., & Chenari, R. J. (2024). Modulus reduction and damping characteristics of geotextile-reinforced sands. Soil Dynamics and Earthquake Engineering, 181, 108641.

[13] Singh, M., Trivedi, A., & Shukla, S. K. (2022). Evaluation of geosynthetic reinforcement in unpaved road using moving wheel load test. Geotextiles and Geomembranes, 50(4), 581-589.

[14] Tsai, C. C., Lin, C. Y., Dashti, S., & Kirkwood, P. (2021). Influence of centrifuge container boundaries and loading characteristics on evaluation of dynamic properties in dry sand. Soil Dynamics and Earthquake Engineering, 142, 106567.

[15] Vrettos, C., & Banzibaganye, G. (2022). Effects of specimen size and inertia on resonant column tests applied to sands. Soil Dynamics and Earthquake Engineering, 155, 107136.

[16] Wang, Y., Li, S., Duan, G., Yin, J., & Wang, Y. (2023). Study on dynamic properties of ultrasoft clay based on large amplitude oscillatory shear tests. Soil Dynamics and Earthquake Engineering, 172, 107989.

[17] Wu, M., Tian, W., Liu, F., & Yang, J. (2023). Dynamic behavior of geocell-reinforced rubber sand mixtures under cyclic simple shear loading. Soil Dynamics and Earthquake Engineering, 164, 107595.

[18] Zou, X., Yang, Z., & Wu, W. (2023). Horizontal dynamic response of partially embedded single pile in unsaturated soil under combined loads. Soil Dynamics and Earthquake Engineering, 165, 107672.

[19] Kumar, Y., Trivedi, A., & Shukla, S. K. (2025). Impact of Moving Load Vibrations on Pavement Damage Supported by Flow-Controlled Geomaterials. *International Journal of Non-Linear Mechanics*, 105045.

[20] El-Khoury, O., & Adeli, H. (2013). Recent advances on vibration control of structures under dynamic loading. *Archives of Computational Methods in Engineering*, *20*, 353-360.

[21] Zhang, Q. B., Liu, K., Wu, G., & Zhao, J. (2022). Dynamic deformation, damage, and fracture in geomaterials. In *Handbook of Damage Mechanics: Nano to Macro Scale for Materials and Structures* (pp. 379-422). Cham: Springer International Publishing.

[22] Sweta, K., & Hussaini, S. K. K. (2022). Role of particle breakage on damping, resiliency and service life of geogrid-reinforced ballasted tracks. *Transportation Geotechnics*, *37*, 100828.

List of publication

1. Pawar, N., Kumar, Y., and Trivedi, A. (2025). Role of geogrid reinforcement of stiffness capacity of loose cohesionless geomaterial. In *Third International Conference on Transportation Infrastructure Projects: Conception to Execution*.
2. Pawar, N., Kumar, Y., and Trivedi, A. (2025). Effect of geogrid reinforcement on the unpaved surface of cohesionless geomaterial. In *Third International Conference on Transportation Infrastructure Projects: Conception to Execution*.